DYNAMIC PHASE TRANSITION IN THE KINETIC SPIN-3/2 BLUME–EMERY–GRIFFITHS MODEL: PHASE DIAGRAM IN THE TEMPERATURE AND INTERACTION PARAMETERS PLANES*

Mustafa Keskin, Bayram Deviren, Osman Canko
Muharrem Kirak

Department of Physics, Erciyes University, 38039 Kayseri, Turkey

(Received December 27, 2006; revised version received February 27, 2007)

As a continuation of our previously published work, the dynamic phase transitions are studied, within a mean-field approach, in the kinetic spin-3/2 Blume–Emery–Griffiths (BEG) model in the presence of a time varying (sinusoidal) magnetic field by using the Glauber-type stochastic dynamics. The dynamic phase transitions (DPTs) are obtained and the phase diagrams are constructed in two different planes, namely reduced temperature (T) and biquadratic interaction (k), (T, k) plane where found seven fundamental types of phase diagrams for both positive and negative values of crystal-field interaction (d) and magnetic field amplitude (h), and also (T, d) plane in which obtained ten distinct topologies for different values of k and h. Phase diagrams exhibit one or two dynamic tricritical points, a dynamic double critical end point, and besides a disordered and two ordered phases, seven coexistence phase regions exist in which occurring of all these strongly depend on the values of k, d and h.

PACS numbers: 05.50.+q, 05.70.Fh, 64.60.Ht, 75.10.Hk

1. Introduction

In a preceding paper [1], we have presented a study within a mean-field approach of the stationary states of the kinetic spin-3/2 Blume–Emery–Griffiths (BEG) model under a time-dependent oscillating external magnetic field. We use the Glauber-type stochastic dynamics [2] to describe the time evolution of the system. We have investigated the time variations of the average order parameters, namely magnetization and quadrupole moment. We have also studied the behavior of the order parameters in a period, which

* Presented at the XIII Ankara Condensed Matter Physics Conference, METU, Turkey, November 3, 2006.

are also called dynamic order parameters, as a function of the reduced temperature. The DPT points are found by investigating the behavior of the dynamic order parameters as a function of the reduced temperature. These investigations are also checked and verified by calculating the Liapunov exponents. Finally, we have presented the phase diagrams in the reduced temperature and magnetic field amplitude plane and found seventeen distinct topologies for several values of the interaction parameters. The phase diagrams exhibit one or two dynamic tricritical points, a dynamic double critical end point, and besides a disordered and two ordered phases, seven coexistence phase regions exist in which occurring of all these strongly depend on interaction parameters. On the other hand, one should study phase diagrams of the model in the reduced temperature (T) and biquadratic pair interaction (k) plane, and in the reduced temperature (T) and crystal-field interaction (d) plane. Therefore, the aim of this paper is to calculate the phase diagrams of the kinetic spin-3/2 BEG model in the presence of a time varying (sinusoidal) magnetic field in the (T, k) and (T, d) planes by using the Glauber-type stochastic dynamics.

It is worthwhile to mention that the physics of the equilibrium phase transition is now rather well understood [3] within the framework of the equilibrium statistical physics. However, the study of nonequilibrium critical phenomena is not presently as well understood either theoretically or experimentally as the equilibrium case due to the complexity. Therefore, further efforts on these challenging time-dependent problems should promise to be rewarding in future. Some interesting problems in nonequilibrium systems are the nonequilibrium or the DPT and it is the one of the most important dynamic responses of current interests. The DPT was first found in a study within a mean-field approach of the stationary states of the kinetic spin-1/2 Ising model under a time-dependent oscillating field [4, 5], by using the Glauber-type stochastic dynamics [2], and it was followed by Monte Carlo simulation, which allows the microscopic fluctuations, researches of the kinetic spin-1/2 Ising models [6], as well as further mean-field studies [7]. Tutu and Fujiwara [8] developed the systematic method for getting the phase diagrams in DPTs, and constructed the general theory of DPTs near the transition point based on mean-field description, such as Landau's general treatment of the equilibrium phase transitions. The DPT has also been found in a one-dimensional kinetic spin-1/2 Ising model with boundaries [9]. Recent researches on the DPT are widely extended to more complex systems such as vector-type order parameter systems, *e.g.*, the Heisenberg-spin systems [10], XY model [11], a Ziff–Gulari–Barshad model for CO oxidation with CO desorption to periodic variation of the CO pressure [12] and a high-spin Ising models such as the kinetic spin-1 [13] and spin-3/2 [14] Ising systems. Moreover, experimental evidences for the DPT have been found in highly anisotropic (Ising-like) and ultrathin Co/Cu(001) ferromagnetic films [15] and in ferroic systems (ferromagnets, ferroelectrics and ferroelastics) with pinned domain walls [16].

The outline of the remaining part of this paper is as follows: In Section 2, the spin-3/2 BEG model is presented and the derivation of the mean-field (MF) dynamic equations is given by using the Glauber-type stochastic dynamics in the presence of a time-dependent oscillating external magnetic field, briefly. In Section 3, the dynamic phase transition points are calculated, and the calculated phase diagrams are presented in the $(T,\ k)$ and $(T,\ d)$ planes. Finally, a conclusion is given in Section 4.

2. The model and derivation of mean-field dynamic equations

Since the model and method, which are derivation of mean-field dynamical equations of motion, were described extensively in [1]; therefore, we shall only give a brief summary in here. The most general spin-3/2 Ising model Hamiltonian with bilinear (J) and biquadratic (K) nearest-neighbor pair interactions and a single-ion potential or crystal-field interaction (Δ) is the spin-3/2 Blume–Emery–Griffiths model and it has been paid much attention for many years. The model is described by the following Hamiltonian:

$$H=-J\sum_{\langle ij\rangle}S_iS_j-K\sum_{\langle ij\rangle}\left(S_i^2-\tfrac{5}{4}\right)\left(S_j^2-\tfrac{5}{4}\right)-\Delta\sum_{i}\left(S_i^2-\tfrac{5}{4}\right)-H\sum_{i}S_i\,, \quad (1)$$

where the S_i takes the value $\pm 3/2$ or $\pm 1/2$ at each i site of a lattice and the summation index $\langle ij\rangle$ denotes a summation over all pairs of neighboring spins. J and K are, respectively, the nearest-neighbor bilinear and biquadratic exchange constants, Δ is the crystal field interaction or single-ion anisotropy constant, and the last term, H, is a time-dependent external oscillating magnetic field. H is given by $H(t)=H_0\cos(\omega t)$, H_0 and $\omega=2\pi\nu$ are the amplitude and the angular frequency of the oscillating field, respectively. The system is in contact with an isothermal heat bath at absolute temperature.

The spin-3/2 BEG model is also three-order parameters system; these are introduced as follows: (1) the average magnetization $m\equiv\langle S_i\rangle$, which is the excess of one orientation over the other orientation, also called the dipole moment. (2) The quadrupole moment q, that is a linear function of the average squared magnetization, *i.e.* $q\equiv\langle S_i^2\rangle-5/4$. This definition ensures that $q=0$ at infinite temperature. (3) The octupolar moment r, which is an odd function of the average magnetization $\langle S_i\rangle$ and defined as $r\equiv 5/3\langle S_i^3\rangle-41/12\langle S_i\rangle$. This definition also ensures that $r=0$ at infinite temperature. We should also mention that since the behavior of r is similar to the behavior of s, we will not use r as many researchers have done.

The system evolves according to a Glauber-type stochastic process at a rate of $1/\tau$ transitions per unit time. We define $P(S_1, S_2, ..., S_N; t)$ as the probability that the system has the S-spin configuration, $S_1, S_2, ..., S_N$, at time t. The time-dependence of this probability function is assumed to be governed by the master equation which describes the interaction between spins and heat bath, and can be written as

$$\frac{d}{dt}P(S_1,S_2,...,S_N;t) = -\sum_i \Big(\sum_{S_i \neq S_i'} W_i(S_i \to S_i') \Big) P(S_1, S_2, ..., S_i, ..., S_N; t) + \sum_i \Big(\sum_{S_i \neq S_i'} W_i(S_i' \to S_i) \Big) P(S_1, S_2, ..., S_i, ..., S_N; t), \quad (2)$$

where $W_i(S_i \to S_i')$, the probability per unit time that the ith spin changes from the value S_i to S_i', and in this sense the Glauber model is stochastic. Since the system is in contact with a heat bath at absolute temperature T_A, each spin can change from the value S_i to S_i' with the probability per unit time

$$W_i(S_i \to S_i') = -\frac{1}{\tau} \frac{\exp(-\beta \Delta E(S_i \to S_i'))}{\sum_{S_i'} \exp(-\beta \Delta E(S_i \to S_i'))}, \quad (3)$$

where $\beta = 1/k_{\mathrm{B}} T_A$, k_{B} is the Boltzmann factor, $\sum_{S_i'}$ is the sum over the four possible values of S_i', $\pm 3/2$, $\pm 1/2$ and ΔE is the change in the energy of the system when the S_i-spin changes that can be obtained by using Eq. (1).

By using the Glauber-type stochastic dynamics, we obtain the set of the mean-field dynamical equations for the average order parameters [1]

$$\Omega \frac{d}{d\xi} m = -m + \frac{3\exp(a/T)\sinh(3b/2T) + \exp(-a/T)\sinh(b/2T)}{2\exp(a/T)\cosh(3b/2T) + 2\exp(-a/T)\cosh(b/2T)}, \quad (4)$$

$$\Omega \frac{dq}{d\xi} = -q + \frac{\exp(a/T)\cosh(3b/2T) - \exp(-a/T)\cosh(b/2T)}{\exp(a/T)\cosh(3b/2T) + \exp(-a/T)\cosh(b/2T)}, \quad (5)$$

where $m \equiv \langle S \rangle$, $q \equiv \langle S^2 \rangle - 5/4$, $a = d + kq$, $b = m + h \cos\xi$, $\xi = wt$, $T = (\beta z J)^{-1}$, $k = K/J$, $d = \Delta/zJ$, $h = H_0/zJ$, $\Omega = \tau w$. We fixed $z = 4$ and $\Omega = 2\pi$.

3. Dynamic phase transition points and phase diagrams

Since determining of the nonequilibrium or dynamic phase transition (DPT) points are discussed in paper I extensively, we shall only give a brief summary in here. For this purpose, first we have to study the stationary solutions of the dynamic equations, given in Eqs. (4) and (5), when the parameters T, k, d and h are varied. The stationary solutions of Eqs. (4)

and (5) will be a periodic function of ξ with period 2π. Moreover, they can be one of three types according to whether they have or do not have the property

$$m(\xi+\pi) \;=\; -m(\xi)\,, \tag{6}$$

and

$$q(\xi+\pi) \;=\; -q(\xi)\,. \tag{7}$$

A solution that satisfies both Eqs. (6) and (7) is called a symmetric solution and corresponds to a disordered (D) solution. In this solution, the magnetization always oscillates around the zero value and is delayed with respect to the external magnetic field. On the other hand, the quadrupolar order parameter $q(\xi)$ oscillates around a nonzero value for finite temperatures and around a zero value for the infinite temperature due to the reason that $q = 0$ at the infinite temperature by the definition of q. The second type of solution does not satisfy Eqs. (6) and (7), and it is called a nonsymmetric solution that corresponds to a ferromagnetic solution. In this case the magnetization and quadrupolar order parameters do not follow the external magnetic field any more, but instead of oscillating around a zero value they oscillate around a nonzero value, namely $m(\xi)$ oscillates around either $\pm 3/2$ or $\pm 1/2$. Hence, if it oscillates around $\pm 3/2$, this nonsymmetric solution corresponds to the ferromagnetic$-3/2$ ($F_{3/2}$) phase and if it oscillates around $\pm 1/2$, this corresponds to the ferromagnetic$-1/2$ ($F_{1/2}$) phase. The third type of solution, which does satisfy Eq. (6) but does not satisfy Eq. (7), corresponds to ferro-quadrupolar or simply quadrupolar (FQ) phase. In this solution, $m(\xi)$ oscillates around the zero value and is delayed with respect to the external magnetic field and $q(\xi)$ does not follow the external magnetic field any more, but instead of oscillating around a zero value; it oscillates around a nonzero value, namely either -1 or $+1$. Hence if it oscillates around -1, this nonsymmetric solution corresponds to the ferro-quadrupolar or simply quadrupolar (FQ) phase, and if it oscillates around $+1$, this corresponds to the disordered phase (D). We have also seven coexistence solutions due to the combination of these solutions or phases. These facts are seen explicitly by solving Eqs. (4) and (5) numerically. Eqs. (4) and (5) are solved by using the numerical method of the Adams–Moulton predictor corrector method for a given set of parameters and initial values. Since the solutions and discussion of the results were given extensively in [1] (see Fig. 1 of Ref. [1]), we will not present the figure in this work. These facts implicitly and Fig. 1 of [1] explicitly show that we have ten phases in the system, namely $D, F_{3/2}, F_{1/2}, F_{3/2}+F_{1/2}, F_{3/2}+D, F_{3/2}+F_{1/2}+FQ, F_{3/2}+FQ, F_{1/2}+FQ, F_{3/2}+FQ+D$ and $FQ+D$.

In order to see the dynamic phase boundaries among these ten phases, we have to calculate DPT points and then we can present phase diagrams

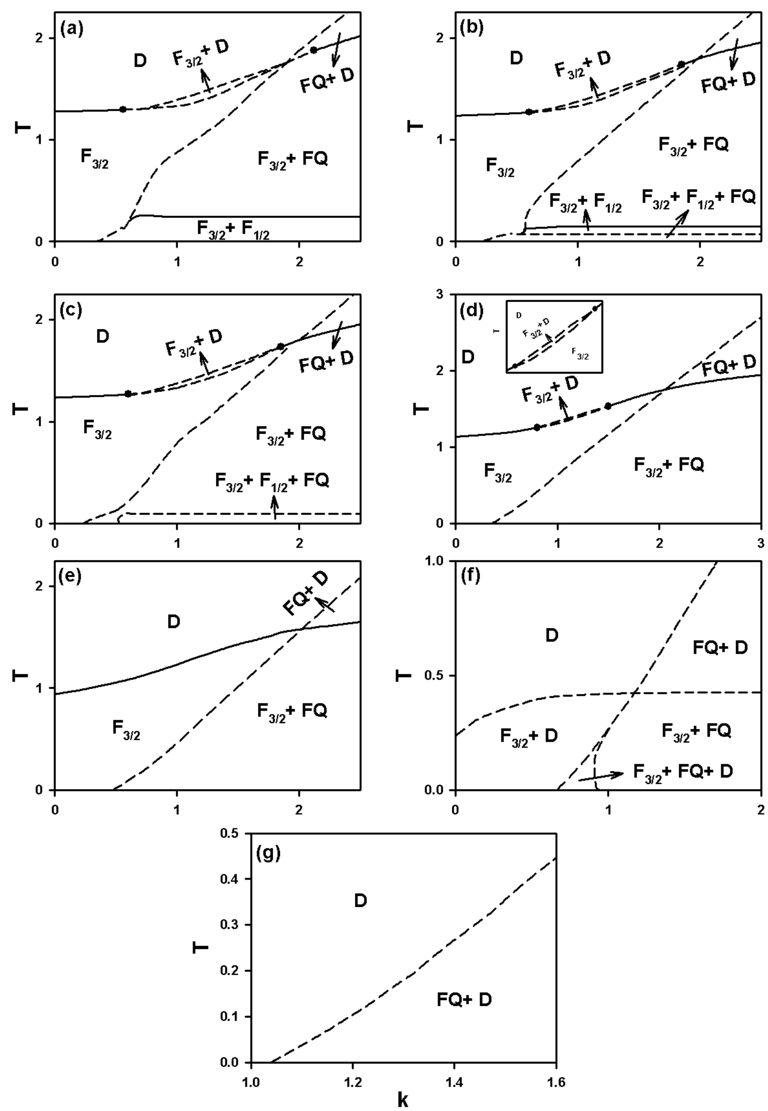

Fig. 1. Phase diagrams of the spin-3/2 BEG model in the $(T,\ k)$ plane for $d \geq 0.0$ ($d = 0.025$) and several values of h. The disordered (D), ferromagnetic-3/2 ($F_{3/2}$), and five different coexistence regions, namely the $F_{3/2} + F_{1/2}$, $F_{3/2} + FQ$, $F_{3/2} + F_{3/2} + FQ$, $F_{3/2} + D$ and $FQ + D$, are found. Dashed and solid lines represent the first- and second-order phase transitions, respectively, and the dynamic tricritical points are indicated with filled circles. (a) $h = 0.125$, (b) $h = 0.35$, (c) $h = 0.375$, (d) $h = 0.625$, (e) $h = 0.875$, (f) $h = 1.25$, and (g) $h = 2.0$.

of the system. DPT points will be obtained by investigating the behavior of the average order parameters in a period or the dynamic order parameters as a function of the reduced temperature. The dynamic order parameters, namely the dynamic magnetization (M) and the dynamic quadruple moment (Q), are defined as

$$M = \frac{1}{2\pi}\int_0^{2\pi} m(\xi)d\xi \qquad \text{and} \qquad Q = \frac{1}{2\pi}\int_0^{2\pi} q(\xi)\,d\xi\,. \tag{8}$$

The behavior of M and Q as a function of the reduced temperature for several values of k, d and h are obtained by combining the numerical methods of Adams–Moulton predictor corrector with the Romberg integration. We will obtain the DPT points and also the type of the phase transition from the behavior of M and Q. For example, if M decreases to zero continuously as the reduced temperature increases, a second-order phase transition occurs at T_{C}. On the other hand, Q decreases until T_{C}, as the temperature increases, and it makes a cusp at T_{C} and then decreases to zero as the temperature increases and it becomes zero at infinite temperature. If M and Q decrease to zero discontinuously, a first-order phase transition occurs, at T_t. Since we gave a few interesting explanatory examples to illustrate the calculation of the DPT and the dynamic phase boundaries among ten phases in Fig. 2 of [1], we will not present any behavior of M and Q in this work. We should also mention that the Liapunov exponents were calculated to verify the stability of solutions and the DPT points in [1], see Fig. 3 there.

We can now present the phase diagrams of the system in the reduced temperature and interaction parameters plane. The calculated phase diagrams are presented in Figs. 1–3 for various values of k, d and h. In these phase diagrams, the solid and dashed lines represent the second- and the first-order phase transition lines, respectively, and the dynamic tricritical point is denoted by a filled circle and B represents the dynamic double critical end point.

Fig. 1 shows the phase diagrams in the $(T,\ k)$ plane for the positive values of d, *i.e.*, $d = 0.025$ and several values of h and the following seven fundamental types of phase diagrams are found. *(i)* Fig. 1(a) represents the phase diagram in the $(T,\ k)$ plane for $h = 0.125$. In this case, besides two dynamic tricritical points, one disordered (D), and one ordered ($F_{3/2}$) and four coexistence regions, namely $F_{3/2} + F_{1/2}$, $F_{3/2} + FQ$, $F_{3/2} + D$ and $FQ + D$, exist in the phase diagram. The dynamic phase boundaries between the D and $F_{3/2}$ phases; between the $F_{3/2} + F_{1/2}$ and $F_{3/2} + FQ$ phases; between the $F_{3/2} + FQ$ and $FQ + D$ phases are second-order lines. All other dynamic phase boundaries among the other phases are first-order lines. *(ii)* This type of the phase diagram is presented for $h = 0.35$, seen in Fig. 1(b).

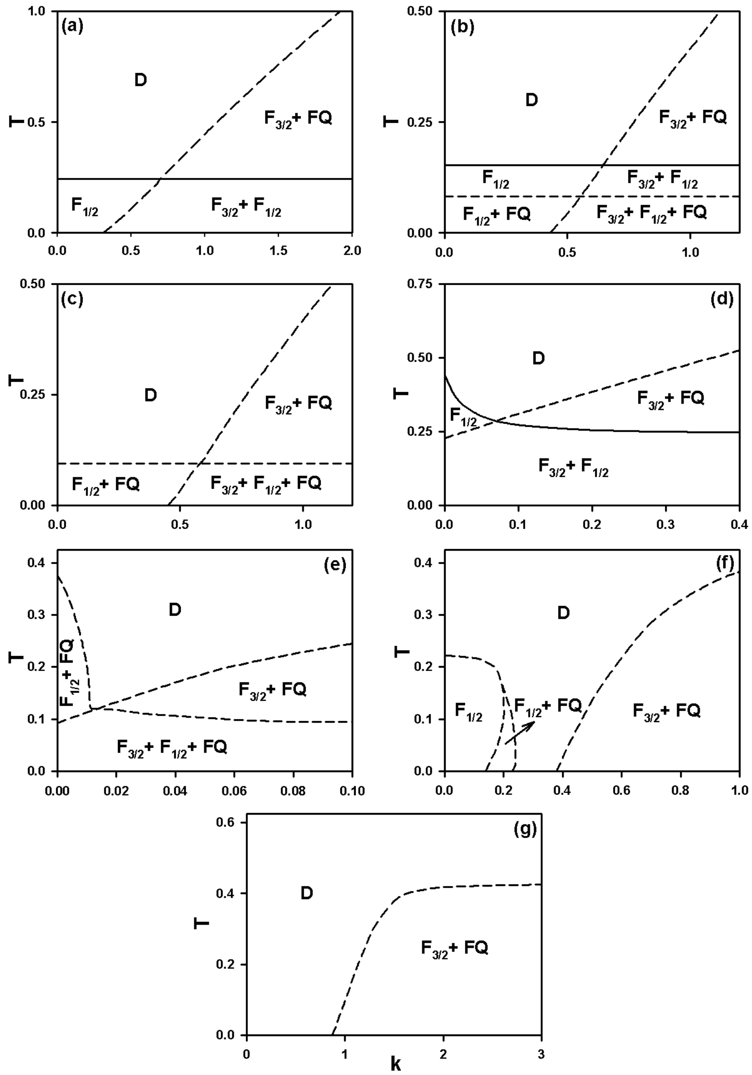

Fig. 2. Phase diagrams of the spin-3/2 BEG model in the $(T,\ k)$ plane for several negative values of d, and h. The disordered (D), ferromagnetic-3/2 $(F_{3/2})$, ferromagnetic-1/2 $(F_{1/2})$ and four different coexistence regions, namely the $F_{3/2}+F_{1/2}$, $F_{3/2}+FQ$, $F_{1/2}+FQ$ and $F_{3/2}+F_{1/2}+FQ$, are found. Dashed and solid lines represent the first- and second-order phase transitions, respectively. (a) $d=-1.0$, $h=0.125$, (b) $d=-1.0$, $h=0.35$, (c) $d=-0.5$, $h=0.125$, (d) $d=-1.0$, $h=0.375$, (e) $d=-0.5$, $h=0.375$, (f) $d=-0.5$, $h=1.25$, and (g) $d=-1.0$, $h=1.25$.

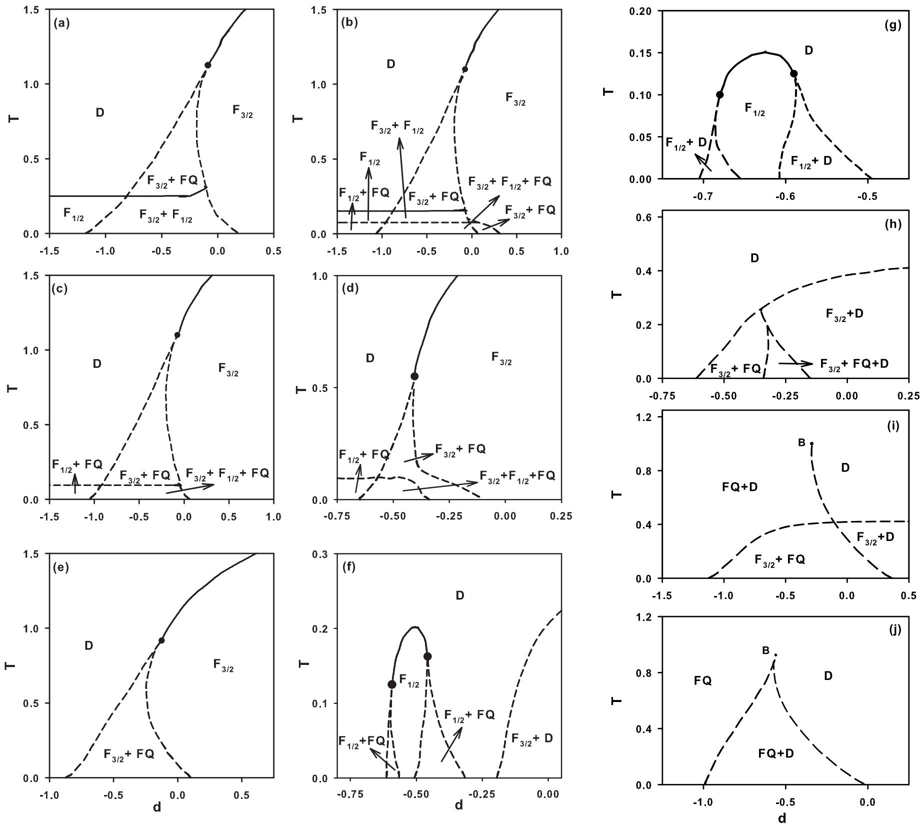

Fig. 3. Phase diagrams of the spin-3/2 BEG model in the (T, d) plane for several values of k and h. The disordered (D), ferromagnetic-3/2 ($F_{3/2}$), ferromagnetic-1/2 ($F_{1/2}$) and seven different coexistence regions, namely the $F_{3/2} + F_{1/2}$, $F_{3/2} + D$, $F_{3/2} + F_{1/2} + FQ$, $F_{3/2} + FQ$, $F_{1/2} + FQ$, $F_{3/2} + FQ + D$ and $FQ + D$, are found. Dashed and solid lines represent the first- and second-order phase transitions, respectively. The dynamic tricritical points are indicated with filled circles, and B denotes the dynamic double critical end point. (a) $k = 0.5$, $h = 0.125$, (b) $k = 0.5$, $h = 0.35$, (c) $k = 0.5$, $h = 0.375$, (d) $k = 0.1$, $h = 0.375$, (e) $k = 0.5$, $h = 0.75$, (f) $k = 0.1$, $h = 1.3$, (g) $k = 0.1$, $h = 1.5$, (h) $k = 0.5$, $h = 1.25$, (i) $k = 1.0$, $h = 1.25$, and (j) $k = 1.0$, $h = 2.0$.

It is similar to Fig. 1(a), the only difference is that in Fig. 1 (a) very low values of T, the $F_{3/2}+F_{1/2}+FQ$ phase or coexistence region also exist. The dynamic phase boundaries between this $F_{3/2} + F_{1/2} + FQ$ and $F_{3/2} + F_{1/2}$ phase, and between the $F_{3/2} + F_{1/2} + FQ$ and $F_{3/2}$ phases are first-order lines. *(iii)* The phase diagram is illustrated in Fig. 1(c) for $h = 0.375$, and it is similar to the case *(ii)*, except that the $F_{3/2} + F_{1/2}$ phase disappears.

(iv) For $h = 0.625$, the phase diagram is presented in Fig. 1(d). While this phase diagram has the same phase topology as the diagram in Fig. 1(c), it only differs from Fig. 1(c) in which the $F_{3/2}+F_{1/2}+FQ$ phase does not occur any more and the $F_{3/2}+D$ phase or coexistence region becomes very small. *(v)* For $h = 0.875$, the calculated phase diagram is illustrated in Fig. 1(e). The system exhibits the D and $F_{3/2}$ phases, and the $F_{3/2}+FQ$ and $FQ+D$ phases. The dynamic phase boundaries between the D and $F_{3/2}$ phases, and between the $F_{3/2}+FQ$ and $FQ+D$ phases are second-order lines. On the other hand, the boundaries between the $F_{3/2}$ and $F_{3/2}+FQ$ phases, and between the D and FQ+D phases are first-order lines. Moreover, the system does not exhibit any dynamic tricritical point. *(vi)* For $h = 1.250$, the phase diagram is seen in Fig. 1(f). In this case, the system exhibits the D phase and the $F_{3/2}+FQ+D$, $F_{3/2}+D$, $F_{3/2}+FQ$, $FQ+D$ coexistence regions. The dynamic phase boundaries among these phases are all first-order lines. *(vii)* This type of the phase diagram is presented for $h = 2.0$, seen in Fig. 1(g) and only the D and $FQ+D$ phases exist. The dynamic phase boundary between these two phases is a first-order phase line. Moreover, at zero and very low values of T, the D phase occurs due to the high values of h.

Fig. 2 displays the phase diagrams in the $(T,\ k)$ plane for the several negative values of d and several values of h, and the following seven fundamental types of phase diagrams are found. *(i)* Fig. 2(a) represents the phase diagram in the $(T,\ k)$ plane for $d = -1.0$ and $h = 0.125$. In this phase diagram, the D, $F_{1/2}$, $F_{3/2}+F_{1/2}$ and $F_{3/2}+FQ$ phases exist. The dynamic phase boundaries between the $F_{1/2}$ and D phases; between the $F_{3/2}+F_{1/2}$ and $F_{3/2}+FQ$ phases are second-order phase lines, but boundaries between the $F_{1/2}$ and $F_{3/2}+F_{1/2}$ phases; between the D and $F_{3/2}+FQ$ phases are first-order lines. *(ii)* This type of the phase diagram is presented for $d = -1.0$ and $h = 0.35$, seen in Fig. 2(b) and this phase diagram is similar to Fig. 2(a), except the following differences: (1) The $F_{1/2}+FQ$ phase exists for low values of T and k. (2) The $F_{3/2}+F_{1/2}+FQ$ phase occurs for low values of T and high values of k. The dynamic phase boundaries between the $F_{1/2}$ and D phases, and between the $F_{3/2}+F_{1/2}$ and $F_{3/2}+FQ$ phases are second-order lines. All the other boundaries among the other phases are first-order lines. *(iii)* For $d = -0.5$ and $h = 0.125$, this type of phase diagram is presented in Fig. 2(c) and it is similar to the case *(ii)*, except that the $F_{1/2}$ and $F_{3/2}+F_{1/2}$ phases disappear. Therefore, the dynamic phase boundaries among all the phases are first-order lines. *(iv)* The phase diagram is obtained for $d = -1.0$ and $h = 0.375$, illustrated in Fig. 2(d). While this phase diagram has the same phase topology as the diagram in Fig. 2(a), it only differs from Fig. 2(a) in which the $F_{1/2}$ phase does not exist for very low values of T and k; but this phase occurs in certain range of T and for the low values of k. *(v)* We performed the phase diagram for $d = -0.5$ and $h = 0.375$, shown in Fig. 2(e). This phase diagram is similar to Fig. 2(c), except that the $F_{1/2} + FQ$ phase does not exist at zero and at very low values of T, and it occurs in certain range of T values; hence the $F_{3/2} + F_{1/2} + FQ$ phase exists at zero and at very low values of T. *(vi)* In this case, the phase diagram is constructed for $d = -0.5$ and $h = 1.25$, seen in Fig. 2(f). In this phase diagram, $F_{1/2}$ phase exists for very low values of T and k, and as the values of k increase, the $F_{1/2} + FQ$ occurs, then the D phase, and finally the $F_{3/2} + FQ$ phase appear, seen in Fig. 2(f). The phase boundaries among all these phases are first-order lines. *(vii)* The phase diagram is constructed for $d = -1.0$ and $h = 1.25$ and presented in Fig. 2(g) and only the D and $F_{3/2} + FQ$ phases exist in which the dynamic phase boundary between these two phases is a first-order phase line. Moreover, the D phase occurs at zero and very low values of T due to the high values of h.

Finally, Fig. 3 shows the phase diagrams in $(T,\ d)$ plane for several values of k and h and the following ten fundamental types of phase diagrams are found. *(i)* We performed the phase diagram for $k = 0.5$ and $h = 0.125$, seen in Fig. 3(a). The phase diagram displays the D, $F_{3/2}$, $F_{1/2}$ phases and the $F_{3/2} + F_{1/2}$, $F_{3/2} + FQ$ coexistence regions or phases. The system also exhibits a dynamic tricritical point. The dynamic phase boundaries between the D and $F_{3/2}$ phases, between the D and $F_{1/2}$ phases, and also between the $F_{3/2}+F_{1/2}$ and $F_{3/2}+FQ$ phases are second-order phase transition lines. The other phase boundaries are all first-order lines. *(ii)* The phase diagram is constructed for $k = 0.5$ and $h = 0.35$, and this phase diagram is similar to Fig. 3(a), except three more coexistence phases, namely the $F_{1/2} + FQ$, $F_{3/2} + F_{1/2} + FQ$ and $F_{3/2} + FQ$, which occur for very low values of T, seen in Fig. 3(b). The dynamic boundaries among the coexistence phases are all first-order lines, except the boundaries between the D and $F_{3/2}$ phases, between the D and $F_{1/2}$ phases, and between the $F_{3/2} + F_{1/2}$ and $F_{3/2} + FQ$ phases which are second-order lines. *(iii)* We have presented the phase diagram for $k = 0.5$ and $h = 0.375$, seen in Fig. 3(c). While this phase diagram has the same phase topology as the diagram in Fig. 3(b), it only differs from Fig. 3(b) in which the $F_{1/2}$, $F_{3/2}+F_{1/2}$ and one of the $F_{3/2}+FQ$ phases do not occur any more, hence the second-order phase line that occurs at low values of T, now disappears. The dynamic boundaries among the other phases are first-order lines, except the boundary between the D and $F_{3/2}$ phases, this boundary is a second-order line. *(iv)* The phase diagram is illustrated for $k = 0.1$ and $h = 0.375$, seen in Fig. 3(d), and it is similar to the case *(iii)*, except that the $F_{1/2} + FQ$ and $F_{3/2} + F_{1/2} + FQ$ phases become smaller; hence the $F_{3/2} + FQ$ phase exists for low values of T and certain range of d values. *(v)* We performed the phase diagram for $k = 0.5$ and $h = 0.75$, shown in Fig. 3(e). This phase diagram is similar to Fig. 3(d), except that the $F_{1/2} + FQ$ and $F_{3/2} + F_{1/2} + FQ$ phases do not exist any more. Moreover, Fig. 3(a)–(e) exhibit a dynamic tricritical point. *(vi)* The phase diagram is for $k = 0.1$ and $h = 1.3$, illustrated in Fig. 3(f). This is a more interesting phase diagram in which the system exhibits two dynamic tricritical points besides the D, $F_{1/2}$, $F_{1/2} + FQ$ and $F_{3/2} + D$ phases. The $F_{3/2} + D$ phase occurs for high values of d and two $F_{1/2} + FQ$ phases exist for low values of d. The dynamic boundary between the D and $F_{1/2}$ phases is a second-order, and other boundaries among the other phases are all first-order lines. *(vii)* In this case, the phase diagram is constructed for $k = 0.1$ and $h = 1.5$, seen in Fig. 3(g). The phase diagram is similar to the Fig. 3(f), except following two differences: (1) the $F_{3/2} + D$ phase disappears; (2) the $F_{1/2} + D$ phases appear instead of the $F_{1/2} + FQ$ phases. Hence, the system exhibits two dynamic tricritical points and besides the D and $F_{1/2}$ phases, only two $F_{1/2} + D$ coexistence regions exist. *(viii)* In this case, the phase diagram is presented for $k = 0.5$ and $h = 1.25$, shown in Fig. 3(h). The system exhibits the D, $F_{3/2} + D$, $F_{3/2} + FQ$ and $F_{3/2} + FQ + D$ phases. The dynamic phase boundaries among these phases are all first-order lines. *(ix)* The phase diagram is calculated for $k = 1.0$ and $h = 1.25$, illustrated in Fig. 3(i). The phase diagram is similar to Fig. 3(h) but following differences have been found: (1) The $FQ + D$ coexistence region occurs for very low values of T and d. (2) The $F_{3/2} + FQ + D$ phase disappears. (3) The system exhibits a dynamic double critical (B) end point where two phases coexist, namely, the $FQ + D$ and D phases. *(x)* We performed the phase diagram for $k = 1.0$ and $h = 2.0$, seen in Fig. 3(j). In the phase diagram, the D, FQ and $FQ + D$ phases exist and the boundaries among these phases are all first-order lines. The system also exhibits a dynamic double critical end point.

4. Conclusion

We present a study, within a mean-field approach, the kinetics spin-3/2 BEG model under a time-dependent oscillating external magnetic field. The kinetics is described by the Glauber-type stochastic dynamics. The dynamic phase transition (DPT) points are obtained by investigating the behavior of the dynamic magnetization and dynamic quadruple moment as a function of the reduced temperature. We found the behavior of the system strongly depends on the values of h and the interactions parameters, namely, d and k. The phase diagrams are constructed in the $(T,\ k)$ and $(T,\ d)$ planes and disordered, two ordered and seven coexistence phase regions are found. In the $(T,\ k)$ plane, we found fourteen fundamental types of phase diagrams for different values of d in which seven is for positive values of d and seven is for negative values of d. On the other hand, we obtained ten different topologies of phase diagram in the (T, d) plane for different values of k and h. The phase diagrams exhibit one or two dynamic tricritical points and also a dynamic double critical end point which occuring of these depend on k, d and h values. The stability of the solutions and the DPT points are checked by calculating the Liapunov exponents.

This work was supported by the Scientific and Technological Research Council of Turkey (TÜBİTAK) Grant No. 105T114 and Erciyes University Research Funds, Grant No. FBA-06-01. Bayram Deviren would like to express his gratitude to the TÜBİTAK for the PhD scholarship.

REFERENCES

[1] O. Canko, B. Deviren, M. Keskin, *J. Phys.: Condens. Matter* **18**, 6635 (2006) and references therein.

[2] R.J. Glauber, *J. Math. Phys.* **4**, 294 (1963).

[3] See, *e.g.*, H.E. Stanley, *Introduction to the Phase Transitions and Critical Phenomena*, Oxford University Press, Qxford 1971; S.K. Ma, *Modern Theory of Critical Phenomena* W.A. Benjamin, Inc., Reading 1976.

[4] T. Tomé, M.J. de Oliveira, *Phys. Rev.* **A41**, 4251 (1990).

[5] J.F.F. Mendes, E.J.S. Lage, *J. Stat. Phys.* **64**, 653 (1991).

[6] See, *e.g.*, A. Chatterjee, B.K. Chakrabarti, *Phys. Rev.* **E67**, 046113 (2003); G. Korniss, P.A. Rikvold, M.A. Novotny, *Phys. Rev.* **E66**, 056127 (2002); A. Krawiecki, *Int. J. Mod. Phys.* **B19**, 4769 (2005).

[7] See, *e.g.* H. Fujisaka, H. Tutu, P.A. Rikvold, *Phys. Rev.* **E63**, 036109 (2001) and references therein.

[8] H. Tutu, N. Fujiwara, *J. Phys. Soc. Jpn.* **73**, 2680 (2004).

[9] M. Khorrami, A. Aghamohammadi, *Phys. Rev.* **E65**, 056129 (2002).

[10] H. Jang, M.J. Grimson, *Phys. Rev.* **E63**, 066119 (2001); H. Jang, M.J. Grimson, C.K. Hall *Phys. Rev.* **B67**, 094411 (2003); H. Jang, M.J. Grimson, C.K. Hall *Phys. Rev.* **E68**, 046115 (2003).

[11] T. Yasui, H. Tutu, M. Yamamoto, H. Fujisaka, *Phys. Rev.* **E66**, 036123 (2002); **67**, 019901(E) (2003).

[12] E. Machado, G.M. Buendía, P.A. Rikvold, R.M. Ziff, *Phys. Rev.* **E71**, 016120 (2005).

[13] M. Keskin, O. Canko, Ü. Temizer, *Phys. Rev.* **E72**, 036125 (2005); M. Keskin, O. Canko, E. Kantar, *Int. J. Mod. Phys.* **C17**, 1239 (2006).

[14] M. Keskin, O. Canko, B. Deviren, *Phys. Rev.* **E74**, 011110 (2006); M. Keskin, O. Canko, M. Kırak, *J. Stat. Phys.* **127**, 359 (2007).

[15] Q. Jiang, H.N. Yang, G.C. Wang, *Phys. Rev.* **B52**, 14911 (1995); Q. Jiang, H.N. Yang, G.C. Wang, *J. Appl. Phys.* **79**, 5122 (1996).

[16] W. Kleemann, T. Braun, J. Dec, O. Petracic, *Phase Trans.* **78**, 811 (2005).

[17] B.K. Chakrabarti, M. Acharyya, *Rev. Mod. Phys.* **71**, 847 (1999).

[18] M. Acharyya, *Phys. Rev.* **E56**, 2407 (1997).